4U 1909+07: a Hidden Pearl

I. Kreykenbohm, F. Fürst, L. Barrágan, J. Wilms, R. E. Rothschild, S. Suchy, K. Pottschmidt

Abstract

We present a detailed spectral and timing analysis of the High Mass X-ray Binary (HMXB) 4U 1909+07 with *INTEGRAL* and *RXTE*. 4U 1909+07 is a persistent accreting X-ray pulsar with a period of approximately 605 s. The period changes erratically consistent with a random walk expected for a wind accreting system. *INTEGRAL* detects the source with an average of 2.4 cps (corresponding to 15 mCrab), but sometimes exhibits flaring activity up to 50 cps (i.e. 300 mCrab). The strongly energy dependent pulse profile shows a double peaked structure at low energies and only a single narrow peak at energies above 20 keV. The phase averaged spectrum is well described by a powerlaw modified at higher energies by an exponential cutoff and photoelectric absorption at low energies. In addition at 6.4 keV a strong iron fluorescence line and at lower energies a blackbody component are present. We performed phase resolved spectroscopy to study the pulse phase dependence of the spectral parameters: while most spectral parameters are constant within uncertainties, the blackbody normalization and the cutoff folding energy vary strongly with phase.

Keywords: X-rays: stars – stars: flare – stars: pulsars: individual: 4U 1909+07 – stars: magnetic fields.

1 Introduction

4U 1909+07 (also known as X1908+07) was discovered with the *Uhuru* satellite as 3U 1912+07 [5, in the third Uhuru catalog]. Since then, the source was detected with most X-ray instruments. The nature of the system was, however, not clear for 30 years. Only in 2000, [24] found a stable 4.4 d period in *RXTE* ASM data, which was interpreted as the orbital period of a binary system. The photoelectric absorption was found to vary by a factor of at least 3 with orbital phase [11]. Such a behavior can be well described by a spherical wind model and an inclination of $54° \leq i \leq 70°$, depending on the parameters of the wind model. Furthermore, 4U 1909+07 shows irregular flaring activity due to inhomogeneities in the wind of the donor star, which lead to different accretion rates.

In 2005, [16] detected an OB star in the near infrared at the location of the X-ray source, thus confirming that the system is indeed a High Mass X-ray Binary (HMXB). They estimated the distance to the source to 7 kpc [16].

Using a pointed *RXTE*-PCA observation, [11] discovered a period of ~ 605 s, explained as the pulse period of a rotating neutron star with an offset magnetic axis. [11] were thus able to refine the binary orbit parameters. They obtained $M_\star = 9$–31 $M_\odot$ and $R_\star \leq 22 R_\odot$ for the mass and radius of the companion star assuming the canonical mass of $1.4\,M_\odot$ for the neutron star.

In this paper, we present the data and data reduction methods in Sect. 2. In Sect. 3 we analyze the pulse period evolution and the pulse profiles and in Sect. 4 we address the spectral properties of the source. We summarize and discuss our results in Sect. 5.

2 Data and Observations

We used all publicly available data of 4U 1909+07 from the International Gamma Ray Laboratory [26, *INTEGRAL*] and the Rossi X-ray Timing Explorer [7, *RXTE*].

INTEGRAL has three X-ray science instruments, which provide coverage from 3 keV up to 10 MeV: the imager IBIS/ISGRI [22, 20 keV to 800 keV] with moderate energy resolution and a large effective area, the spectrometer SPI [23, 20 keV to 10 MeV] with excellent spectral resolution suitable for the analysis of nuclear lines, and the X-ray monitor JEM-X [12, 3 keV to 35 keV]. Thanks to ISGRI's large field of view of almost $30° \times 30°$ more than 6 Msec of data on 4U 1909+07 exist, mostly from the *INTEGRAL* core programme [25] and the GRS 1915+105 monitoring [17], however, 4U 1909+07 was almost never in the field of view of JEM-X, as no observations were pointed directly at 4U 1909+07.

Among the detected sources in the field of view are prominent sources like GRS 1915+105 or SS 433. In total, twelve sources with a significance $> 6\sigma$ were detected in the field of view, with 4U 1909+07 being the fourth brightest source. In addition to the standard pipelines of the Offline Scientific Analysis software (OSA) version 7.0 for images and spectra, the `ii_light` distributed with OSA was used to obtain light curves with a higher temporal resolution. We used a time resolution of 20 s to maintain

an acceptable signal-to-noise ratio and to obtain a good enough time resolution to measure the pulse period.

In addition to the *INTEGRAL* observations, we also used the observations of 4U 1909+07 performed by RXTE. Both major instruments of *RXTE*, the Proportional Counter Array [6, PCA], sensitive in the 2–60 keV energy band and the High Energy X-Ray Timing Experiment [18, HEXTE], sensitive between 15–250 keV, were fully operational at that time. Both instruments have a large effective area and a high temporal resolution, but no imaging capabilities. In total, 196 ksec of *RXTE* data on 4U 1909+07 are available.

3   Timing analysis

3.1   Pulse period evolution

Apart from the discovery of the pulsations based on *RXTE* data in 2000 and 2004 [11], no other measurements of the pulse period of 4U 1909+07 are available. The extensive archival *INTEGRAL* data are therefore optimal to track the evolution of the pulse period since 2003. We split the lightcurve into segments between 300 ksec and 800 ksec length to determine the period accurately. We then used epoch folding [10] to determine the pulse period for each of these segments individually. 4U 1909+07 shows very strong pulse-to-pulse variations such that the actual pulse cannot be seen by the naked eye (see, e.g., Figure 1). Only after folding 500–1 000 pulses, a stable pulse profile emerges which allows for a reliable pulse period determination. The pulse profile itself, however, is remarkably stable on longer time scales. A similar effect is seen in Vela X-1, although the overall luminosity is much higher in that source [20].
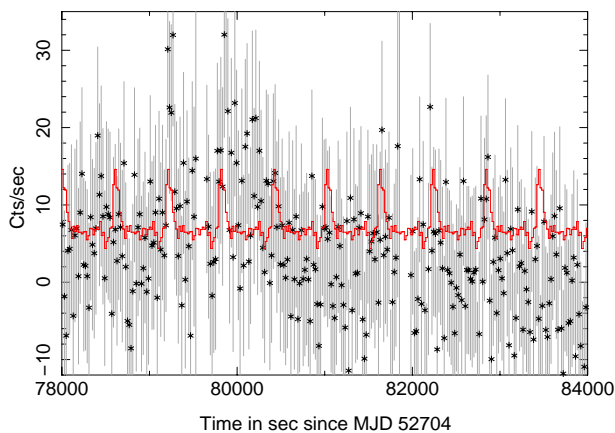
The evolution of the pulse period since 2001 is shown in Figure 2. The overall behavior is best described by a random walk model, but also a spin-up trend between March 2003 and April 2006 and a spin-down trend from April 2006 to October 2007 could describe the data. To confirm the random walk behavior, we implemented the algorithm proposed by [2]: this algorithm evaluates the relative change in the pulse period P over different time intervals δt between individual measurements. In the case of a perfect random walk, the result will be a straight line with a slope of 0.5 in the $\log \delta \omega - \log \delta t$ space, where ω is the angular velocity: $\omega = 2\pi/P$. Figure 3 shows the corresponding diagram for 4U 1909+07. Superimposed is a line with a slope of 0.5, shifted in y-direction to fit the data. It is obvious that the line matches the data very well. The uncertainties in Figure 3 include uncertainties of the determined pulsed periods and also the uneven and coarse sampling.
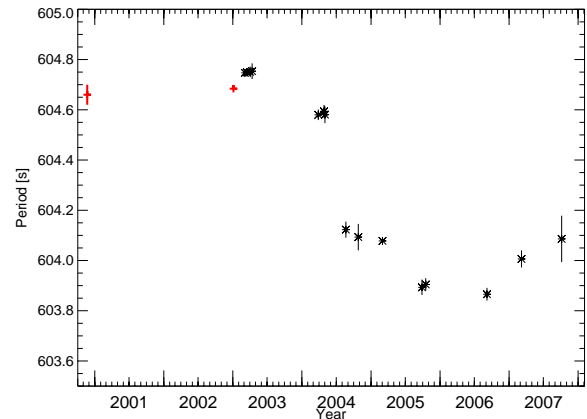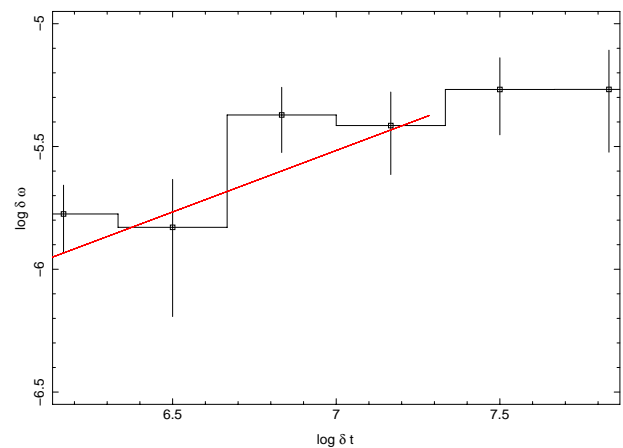

Fig. 2: Evolution of the pulse period of 4U 1909+07. The historic *RXTE* data points of [11] are shown as red crosses, our measurements obtained with *INTEGRAL* are shown as stars
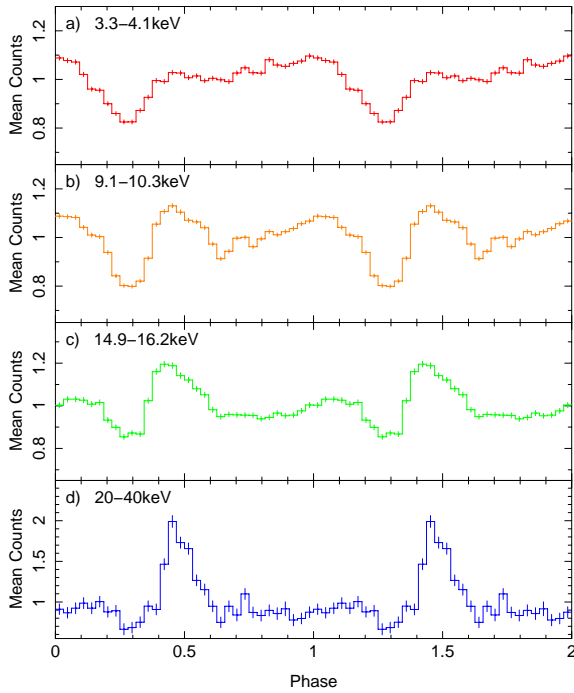

Fig. 1: Closeup on an ISGRI lightcurve of 4U 1909+07 in the 20–40 keV with 20 s time resolution. The red line shows the folded pulse profile

Fig. 4: Energy resolved pulse profiles with *RXTE* PCA (**a**–**c**) and *INTEGRAL* ISGRI (**d**). The profiles are shown twice for clarity. Note that the *RXTE* and *INTEGRAL* profiles are not strictly phase aligned

3.2 Pulse profiles

As shown by [11], the 3.7–17 keV pulse profile shows two distinct peaks, with the second peak being slightly broader than the first peak and having a complex shape with two subpeaks at phase $\phi = 0.85$ and $\phi = 0.1$. To study the energy dependence of the pulse profile, we extracted pulse profiles from PCA data in different energy bands, using a period of $P = 604.685$ s and 32 phase bins. Thanks to the large effective area of the PCA instrument, high quality pulse profiles could be extracted in 30 narrow energy bands. Three energy bands are shown as an example in the upper three panels of Figure 4. The pulse profiles show a smooth transition from a two peaked profile at low energies to a single peak profile at high energies. At energies below 5 keV the secondary peak is broader and stronger than the primary peak (Figure 4a). With increasing energy both peaks become at first equally strong and more clearly separated and then the relative strength of the secondary peak declines further (Figure 4b,c). To obtain the pulse profile at high energies between 20 keV and 40 keV, we used *INTEGRAL* data taken in 2004. We used the same epoch as for the PCA analysis, but a period of $P = 604.747$ s, as determined by our analysis of the *INTEGRAL* data. In this energy band, the secondary peak does not exist anymore while the primary pulse is clearly seen and has a sharp peak (Figure 4d). The deep mini-mum around phase 0.3, however, is not energy dependent.

4 Spectral analysis

4.1 Phase averaged spectrum

The pulse phase averaged spectrum of 4U 1909+07 is best described by a powerlaw continuum attenuated by photoelectric absorption at low energies and an exponential turnover at high energies similar to most accreting X-ray pulsars. [11] modeled the spectrum using bremsstrahlung, which describes the data equally well. The turnover at high energies is often modeled with `cutoffpl`, `highecut`, or the `fdcut` [21]. The `npex` model [15] is more complex as it involves a second powerlaw. Furthermore at 6.4 keV an iron fluorescence line is present.

We discarded all observations between orbital phase $0.88 < \phi_{\rm orb} < 0.12$, as the $N_{\rm H}$ is dramatically increased during this part of the orbit [11]. We applied the typical continuum models (see above) to the *RXTE* and *INTEGRAL* data (see Table 1). All models can describe the data almost equally well. In the case of the `fdcut` model, however, the cutoff energy is set to < 1 keV, thus effectively removing the cutoff. We therefore did not use the `fdcut` model any more for 4U 1909+07. Independent of the applied continuum models, however, a soft excess below 10 keV is evident, which can be very well modeled using a blackbody with a temperature of $kT \approx 1.4$ keV. Figure 5 shows the spectrum and the best fit `cutoffpl` model.

4.2 Phase resolved spectra

Since the *INTEGRAL* ISGRI data did not provide high enough statistics for high resolution phase resolved spectroscopy, we only used the *RXTE* data. We divided the PCA and HEXTE data into 7 phase bins (see Figure 6a). We applied a `cutoffpl` with an additional blackbody component to all phase bins. Neither the photoelectric absorption nor the power law index Γ varies with pulse phase. The cutoff folding energy, however, is highest in the primary peak with ~ 19 keV, while it is only ~ 14 keV during the secondary peak, explaining why the primary peak is much stronger at higher energies.

The blackbody component is strongly variable: the normalization changes by a factor of ~ 3. The blackbody is strongest between the two peaks and weakest in the rise and maximum of the primary peak. The temperature kT of the blackbody on the other hand does not change with pulse phase.

The width of the iron line $\sigma_{\rm Fe}$ is consistent with a narrow line with zero width for most phase bins except during the peak of the pulse where it has a width of ~ 0.4 keV.

Table 1: Fit parameters for various models of the phase averaged spectrum of 4U 1909+07

Model parameter	Cutoffpl	Cutoffpl +bbody	Highecut
$\chi^2_{\rm red}$	1.76	1.01	1.07
$N_{\rm H}$ [10^{22} atoms cm^{-2}]	$15.3^{+0.6}_{-0.5}$	$4.7^{+1.6}_{-1.9}$	$4.8^{+0.9}_{-1.6}$
Γ^1	$1.63^{+0.13}_{-0.02}$	$0.96^{+0.03}_{-0.06}$	$1.37^{+0.03}_{-0.08}$
Fe σ	$1.7^{+0.1}_{-0.5}$	$0.28^{+0.15}_{-0.11}$	$0.41^{+0.07}_{-0.06}$
Fe Energy [keV]	$6.4^{+0.8}_{-0.2}$	$6.40^{+0.04}_{-0.06}$	$6.39^{+0.04}_{-0.03}$
Fe Norm	$(1.1^{+0.1}_{-0.6}) \times 10^{-3}$	$(0.57^{+0.17}_{-0.11}) \times 10^{-3}$	$(0.78^{+0.07}_{-0.04}) \times 10^{-3}$

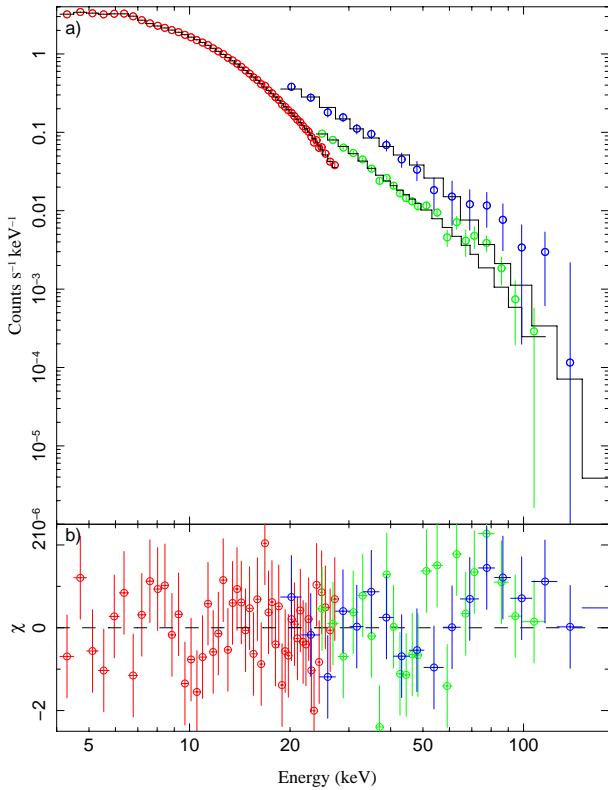| Model parameter	Highecut +bbody	NPEX	NPEX +bbody
$\chi^2_{\rm red}$	0.91	1.44	0.93
$N_{\rm H}$ [atoms cm^{-2}]	$6.8^{+2.0}_{-0.8}$	$1.7^{+0.7}_{-1.7}$	5^{+1}_{-3}
Γ^2	1.32 ± 0.10	$0.36^{+0.05}_{-0.15} \,/\, -3.08^{+0.13}_{-0.09}$	$0.80^{+0.06}_{-0.15} \,/\, -2.0^3$
Fe σ	0.2 ± 0.2	$0.41^{+0.07}_{-0.06}$	$0.27^{+0.12}_{-0.18}$
Fe Energy [keV]	$6.39^{+0.04}_{-0.05}$	$6.37^{+0.04}_{-0.03}$	6.40 ± 0.05
Fe Norm	$(5^{+3}_{-1}) \times 10^{-4}$	$(0.80^{+0.07}_{-0.06}) \times 10^{-3}$	$(0.6^{+0.3}_{-0.1}) \times 10^{-3}$

Fig. 5: **a** Combined *RXTE* PCA (red) and HEXTE (blue) and *INTEGRAL* ISGRI (green) spectrum. The best fit `cutoffpl`-model is also shown. **b** Residuals of the best fit showing no evident deviation

5 Discussion & Conclusion

We have presented a detailed study with *INTEGRAL* and *RXTE* of 4U 1909+07. We have shown that the pulse period changes strongly with time. The evolution of the period is best described by a random walk. Such a behavior has been seen in many other HMXBs like Vela X-1 and is a strong indicator for a direct accretion from the stellar wind of the optical companion without a persistent accretion disk [4]. An accretion disk would provide a more constant transfer of angular momentum and thus a long-term spin-up or spin-down trend, as seen in other sources like 4U 1907+09 [3]. Since the accreting neutron star is strongly magnetized (as indicated by strong coherent pulsations), the accreted matter has to couple to the magnetic field thus inhibiting the formation of an accretion disk close to the neutron star. The required B field strength is of the order of 10^{12} G. Such magnetic field strengths are commonly observed in neutron stars, especially pulsars. In such a strong magnetic field, however, cyclotron resonant scattering features (CRSFs) are expected to be present in the X-ray spectrum, as in the spectrum of Vela X-1 [9] or MXB 0656−072 [13]. Unfortunately, we found no evidence for a CRSF in 4U 1909+07 and are thus unable to determine the strength of the magnetic field. However, the absence of CRSFs in the X-ray spectrum does not rule out the presence of a strong magnetic field in 4U 1909+07, as CRSFs can be filled up again by photon spawning and depend strongly
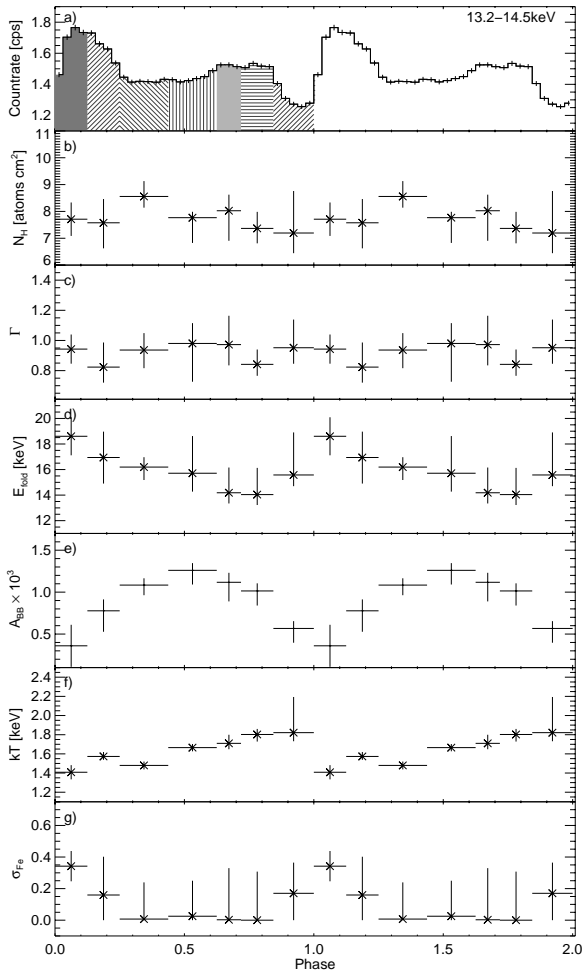
Fig. 6: Spectral parameters of phase-resolved spectra **b** Pulse profile in the 13.2–14.5 keV energy range. The different shaded areas indicate the phase bins. **b** Photoelectric absorption column N_H in units of 10^{22}, **c** Power law index Γ, **d** Folding energy, **e** Blackbody normalization, **f** Blackbody temperature, and **g** width of the Iron line

on the geometry of the accretion column and on the viewing angle [19].

The two distinct peaks in the pulse profile at low energies suggest that the neutron star is accreting on both magnetic poles. However, the dramatic change of the pulse shape with energy suggests that the physical conditions in the accretion columns above the two poles might be different. The exact geometry of the accretion column, however, depends strongly on the way the matter couples to the magnetic field and is highly uncertain [1, 14]. Besides a simple filled funnel other possible configurations exist including a hollow or a partly hollow funnel and several small funnels.

These models, however, have to be taken with a pinch of salt, as the behavior of relativisitc plasma in magnetic fields with $B \approx 10^{12}$ G is still only little understood. Additionally, gravitational light bend-

ing must be taken into account when analyzing pulse profiles and their origin [8].

References

[1] Basko, M. M., Sunyaev, R. A.: *MNRAS*, 1976, **175**, 395.

[2] de Kool, M., Anzer, U.: *MNRAS*, 1993, **262**, 726.

[3] Fritz, S., Kreykenbohm, I., Wilms, J., et al.: *A & A*, 2006, **458**, 885.

[4] Ghosh, P., Lamb, F. K.: *ApJ*, 1979, **234**, 296.

[5] Giacconi, R., Murray, S., Gursky, H., et al.: *ApJS*, 1974, **27**, 37.

[6] Jahoda, K., Markwardt, C. B., Radeva, Y., et al.: *ApJS*, 2006, **163**, 401.

[7] Jahoda, K., Swank, J. H., Giles, A. B., et al.: X-Ray and Gamma-Ray Instrumentation for Astronomy VII, ed. O. H. W. Siegmund, M. A. Gummin, *EUV*, SPIE 2808, 1996, 59–70.

[8] Kraus, U., Zahn, C., Weth, C., Ruder, H.: *ApJ*, 2003, **590**, 424.

[9] Kreykenbohm, I., Coburn, W., Wilms, J., et al.: *A & A*, 2002, **395**, 129.

[10] Leahy, D. A., Darbo, W., Elsner, R. F., et al.: *ApJ*, 1983, **266**, 160.

[11] Levine, A. M., Rappaport, S., Remillard, R., Savcheva, A.: *ApJ*, 2004, **617**, 1 284.

[12] Lund, N., Budtz-Jørgensen, C., Westergaard, N. J., et al.: *A & A*, 2003, **411**, L231.

[13] McBride, V. A., Wilms, J., Coe, M. J., et al.: *A & A*, 2006, **451**, 267.

[14] Meszaros, P.: *Space Sci. Rev.*, 1984, **38**, 325.

[15] Mihara, T.: PhD thesis, RIKEN, Tokio, 1995.

[16] Morel, T., Grosdidier, Y.: *MNRAS*, 2005, **356**, 665.

[17] Rodriguez, J., Bodaghee, A.: *ArXiv e-prints*, 2008, **801**.

[18] Rothschild, R. E., Blanco, P. R., Gruber, D. E., et al.: *ApJ*, 1998, **496**, 538.

[19] Schönherr, G., Wilms, J., Kretschmar, P., et al.: *A & A*, 2007, **472**, 353.

[20] Staubert, R., Kendziorra, E., Pietsch, W. C., Reppin, J. T., Voges, W.: *ApJ*, 1980, **239**, 1 010.

[21] Tanaka, Y.: in *Radiation Hydrodynamics in Stars and Compact Objects*, ed. D. Mihalas, K.-H. A. Winkler, IAU Coll. 89, Heidelberg, 1986, **198**.

[22] Ubertini, P., Lebrun, F., Di Cocco, G., et al.: *A & A*, 2003, **411**, L131.

[23] Vedrenne, G., Roques, J.-P., Schönfelder, V., et al.: *A & A*, 2003, **411**, L63.

[24] Wen, L., Remillard, R. A., Bradt, H. V.: *ApJ*, 2000, **532**, 1 119.

[25] Winkler, C.: in *Exploring the Gamma-Ray Universe*, ed. A. Gimenez, V. Reglero, C. Winkler, ESA SP-459, Alicante, 2001, **471**.

[26] Winkler, C., Courvoisier, T. J.-L., Di Cocco, G., et al.: *A & A*, 2003, **411**, L1.

Ingo Kreykenbohm
E-mail: ingo.kreykenbohm@sternwarte.uni-erlangen.de
Felix Fürst
Laura Barrágan
Jörn Wilms
Dr. Karl Remeis-Sternwarte Bamberg
Sternwartstrasse 7, 96049 Bamberg, Germany
Erlangen Centre for Astroparticle Physics (ECAP)
Erwin-Rommel-Str. 1, 91058 Erlangen, Germany

Richard E. Rothschild
Slawomir Suchy
Center for Astrophysics and Space Sciences
University of California
San Diego, La Jolla, CA 92093-0424, USA

Katja Pottschmidt
CRESST, University of Maryland
Baltimore County
1000 Hilltop Circle, Baltimore, MD 21250, USA
NASA Goddard Space Flight Center
Astrophysics Science Division
Code 661, Greenbelt, MD 20771, USA